ELSEVIER

Journal of Fluids and Structures 25 (2009) 721–730

JOURNAL OF FLUIDS AND STRUCTURES

www.elsevier.com/locate/jfs

Wake dynamics past a curved body of circular cross-section under forced cross-flow vibration

A. de Vecchi*, S.J. Sherwin, J.M.R. Graham

Department of Aeronautics, Imperial College London, SW7 2BT, UK

Received 31 March 2008; accepted 28 January 2009
Available online 31 March 2009

Abstract

Three-dimensional numerical simulations are presented of flow past a curved body at a Reynolds number of 100. The geometry consists of a circular cross-sectioned body, whose centreline axis is prescribed by a quarter ring with a horizontal extension. This plane of curvature of the body is aligned to the free-stream flow direction such that the outer part of the ring is the body's stagnation face (convex configuration). The bluff body is forced to sinusoidally vibrate in the cross-flow direction at different amplitudes and frequencies. The resulting vortex shedding is strongly influenced by the curvature of the body. Within the lock-in region for a straight cylinder, the shedding past the convex body exhibits a 2S mode for all the pairs of input parameters tested; outside this region, a "weak" form of shedding with two pairs of counter-rotating vortices per cycle occurs in the top part of the body. At lower amplitudes of oscillation and frequencies below the Strouhal value for a straight cylinder, dislocations are found in the near wake: these generally occur in the middle of the curved part of the body, at an angle of approximately 45° from the top plane, regardless of the amplitude of oscillation. However, at very low amplitudes, an increase in the input frequency is found to influence the spanwise position of the dislocations by shifting them towards the top sections. The wake dynamics and force distribution are associated with the relative importance of the different regions of the curved geometry: the top region, nearly perpendicular to the inflow and therefore comparable to a straight cylinder, and the lower region with the horizontal extension, which is parallel to the inflow direction and hence behaves similarly to a slender body. The influence of the force contributions from these regions and their different nature determine the occurrence of dislocations in the wake, as well as their position along the span. The energy transfer mechanism, which determines whether the body is excited or damped by the flow, is also affected by this balance: at very low amplitudes the top part undergoes a lift force due to vortex shedding, which is strong enough to overcome the dampening effect from the horizontal extension used in this case and therefore provides a positive energy transfer from the fluid to the structure.

Keywords: Vortex shedding; Curved bluff body; Forced vibration

1. Introduction

A useful approach to understanding and eventually predicting a complex problem like vortex-induced vibration is represented by forced vibration simulations, in which the amplitude and the frequency of motion can be varied

*Corresponding author.
E-mail address: a.devecchi@imperial.ac.uk (A. de Vecchi).

0889-9746/$ - see front matter
doi:10.1016/j.jfluidstructs.2009.01.005

independently. One of the most comprehensive studies on this matter was carried out by Williamson and Roshko (1988), who studied the wake of a circular cylinder forced to move along a sinusoidal path in the range $300 < Re < 1000$ by varying the amplitude and the frequency of oscillation. They identified three principal types of vortex patterns, which characterised different regions of the plane (λ/D, A/D), i.e. a 2S mode (two oppositely signed vortices per cycle), a 2P mode (two pairs of oppositely signed vortices per cycle) and a P + S mode (a single vortex and a pair of vortices per cycle). Two-dimensional numerical computations were not able to reproduce the 2P mode of shedding, probably due to the limitations on the Reynolds number dictated by the computational cost. In their two-dimensional simulations, Meneghini and Bearman (1995) established the lock-in boundary for vortex shedding of a cylinder forced to oscillate in the transverse direction at $Re = 200$. For $A/D < 0.6$, they identified a 2S shedding mode and labelled this kind of synchronisation "primary lock-in". As the amplitude was increased to higher values, the wake presented a P + S mode of shedding, but no evidence of the 2P mode was found. Similarly, the results obtained by Blackburn and Henderson (1999) at $Re = 500$ could successfully reproduce only 2S and P + S modes. More recently, Leontini et al. (2006) generated a parametric map using two-dimensional simulations of a circular cylinder in forced vibration at fixed Reynolds numbers of 100 and 200. They investigated the mechanism behind the formation of the different modes and the direction of the energy transfer: the latter was found to be primarily dependent on frequency at low amplitudes of oscillation but strongly dependent on amplitude at higher amplitudes (i.e. $A/D > 0.4$). The boundaries between positive and negative energy transfer were relatively insensitive to the Reynolds number, which in turn influenced the width of the lock-in region and the wake modes. Ponta and Aref (2005, 2006) presented a theoretical argument to explain the mode transition in the Williamson and Roshko map: the mechanism controlling the formation of different modes was suggested to be dependent on a fine balance of the splitting mechanism (as also discussed by Govardhan and Williamson, 2000) and the level of fluctuation in the shedding frequency played an important role in the transition from a 2P to a P + S mode. Willden et al. (2008) carried out a similar parametric study by means of two-dimensional simulations at $Re = 100$: this is shown in Fig. 1 and used as a reference in the present work. In all these investigations, the 2S mode was found to be predominant in the lock-in region and the P + S mode appeared only at higher amplitudes (i.e. $A/D > 0.8$ for $Re = 100$). One of the first numerical simulations of the 2P mode was performed by Blackburn et al. (2000), who found this mode associated with a double-peaked form in the time-series of the lift coefficient. By comparison with two-dimensional calculations, they demonstrated that three-dimensional computations are required to reproduce the response envelope observed experimentally.

Nuzzi et al. (1992) investigated the vortex formation past a cylinder with a gradual spanwise nonuniformity subjected to transverse controlled oscillations. Globally locked-in states were found to occur along the entire span. At low excitation frequencies, regions of period-doubled vortex formations appeared from the three-dimensional portion of the cylinder, while the straight two-dimensional region maintained a locked-in response: the lock-in region for the nonuniform portion was found to be shifted towards higher input frequencies, at which low-frequency modulations occurred in the straight part. Due to the larger formation length and to the higher phase speed of the instability, the vortex formation from the three-dimensional portion was found to lead that from the two-dimensional part of the

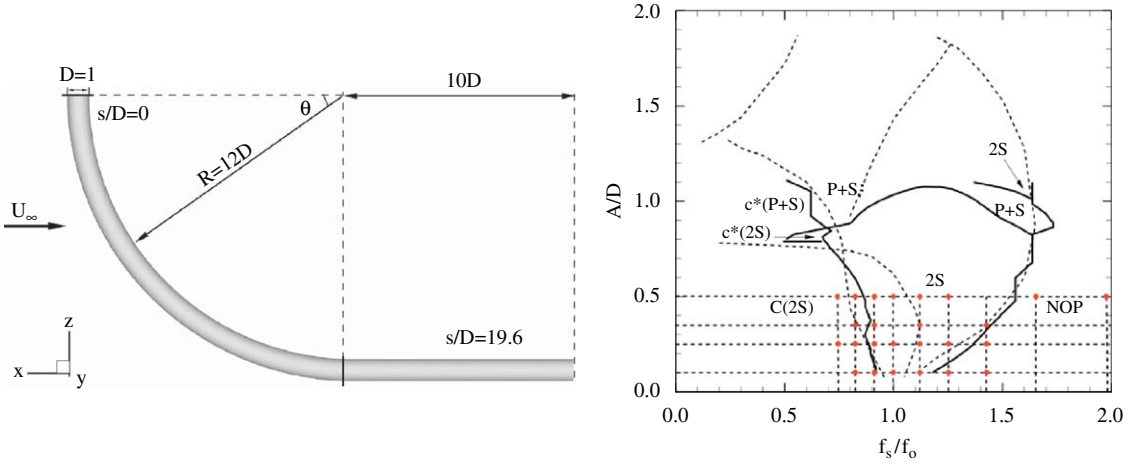

Fig. 1. Left: Sketch of the convex configuration. Right: Map of vortex shedding modes for a tow-dimensional cylinder at $Re = 100$ (Willden et al., 2008) with the flow states analysed in the present simulations.

cylinder. The period-doubled state was characterised by the alternating formation of split and unsplit vortices and dislocations were observed: however, this mode of shedding did not involve vortex coalescence.

Although vortex dislocations are found to be an inherent feature of the three-dimensional wake transition, their presence has also been observed in the laminar vortex shedding regime, where they appeared in a more ordered and periodic fashion than in the transition regime. As observed by Eisenlohr and Ecklemann (1989) and Williamson (1988, 1989), this phenomenon is associated with the presence of oblique shedding and is hence strictly related to the end conditions of the experiments. Williamson (1992) provided experimental evidence that dislocations appear between cells of different frequency and involve vortex splitting, whereby a vortex of one sign in one cell is divided and linked to two vortices of the same sign in the other cell: this mechanism occurs at a beat frequency $f_1 - f_2$, where f_1 and f_2 are the shedding frequencies in the two cells, and involves helical twisting of the vortex lines within a vortex, inducing an axial core flow outwards from the dislocation. The downstream growth of the dislocations is found to cause large velocity fluctuations at low frequency and is associated to the relatively slow decay of fluctuation energy as compared with the laminar wake.

The type of curved geometry presented in this paper was studied for the first time by Miliou et al. (2007), who investigated the vortex shedding past the fixed convex cylinder in a uniform flow. A 2S mode of shedding with straight cores was observed at $\mathrm{Re} = 100$ with only one dominant frequency for the whole body. As a result of the curvature, the distance between the detaching vortex and the cylinder decreased from the top of the quarter ring to the bottom: therefore, the curved stagnation face introduced a gradual phase shift along the span and the influence of the developing shear layers on the body (and subsequently the force distribution) changed accordingly. Since the cylinder was kept fixed, the horizontal extension did not influence the vortex shedding in the curved part and no significant forces were detected in this region.

In the present paper, Section 2 outlines the computational technique and the details of the configuration examined. The effect of the curvature on the type of shedding and on the energy transfer is analysed in Section 3, where the consequences of frequency and amplitude variations are also discussed; a "weak" form of shedding with vortex dislocations is also presented in this section. The occurrence of vortex dislocation is further investigated in Section 4. Finally, a summary of the results and conclusions is given in Section 5

2. Computational technique

The incompressible Navier–Stokes solver employed in the computations throughout this work is the parallel three-dimensional spectral element code *Nεκταr* (Karniadakis and Sherwin, 2005). This is based on the spectral/*hp*-element method for the spatial discretisation, while the temporal accuracy is achieved using a high-order stiffly stable splitting scheme (Karniadakis et al., 1991). The solution at time t_{n+1} is obtained from the solution at t_n over three sub-steps. First, the nonlinear term is treated explicitly, then a Poisson equation for the pressure is obtained by taking the divergence of the pressure term and by enforcing the incompressibility constraint. Finally, the diffusive term is treated implicitly in the last sub-step.

Fig. 1 (left) illustrates the layout of the convex configuration: this is based on a quarter ring whose radius of curvature, $R = 12D$, has been chosen close to the limit value for the flexible pipes used in off-shore applications. The free-stream is aligned to the plane of curvature and the cylinder is forced to oscillate in the transverse direction (y-axis). s/D represents the nondimensional arc-length, with $s/D = 0$ and 19.6 denoting the top and the end of the quarter ring, respectively. Symmetry boundary conditions are assigned to the top plane boundary of intersection with the curved cylinder ($w = 0$, $\mathrm{d}u/\mathrm{d}n \equiv \mathrm{d}u/\mathrm{d}z = 0$ and $\mathrm{d}v/\mathrm{d}n \equiv \mathrm{d}v/\mathrm{d}z = 0$), while a fully developed zero stress condition is imposed at the outflow of the computational domain.

3. Effect of curvature on the energy transfer mechanism

Fig. 1 (right) illustrates the pairs of nondimensional input parameters $(f_s/f_0, A/D)$ investigated in this study, overlaid on the parameter plane obtained by Willden et al. (2008) with two-dimensional simulations at the same Reynolds number of 100. The amplitude of oscillation ranges from a minimum value of $0.1D$ to a maximum of $0.5D$, whereas the input frequency f_0 varies from $0.5f_s$ to $1.3f_s$, where f_s is the Strouhal number for a fixed straight cylinder at $\mathrm{Re} = 100$.

3.1. High amplitudes: hydrodynamic damping from the horizontal extension

At $A/D = 0.5$, the shedding from the top part of the quarter ring is found to be driven by the one in the lower part: the influence of this region is predominant and determines the wake topology further above. Fig. 2 shows the λ_2

iso-surfaces and the sectional distribution of the lift coefficient for $A/D = 0.5$ and $f_0 = 1.1f_s$: the vortical structures are aligned to the cylinder's axis and the lift force is in phase with the body's motion. Its magnitude is markedly higher in the lower half of the quarter ring and in the horizontal extension than at the top: this is an intrinsic feature of this geometry and it has a significant influence on the energy transfer mechanism.

The part of the lift coefficient in phase with the cylinder's velocity, C_{L_v}, is proportional to the energy transferred from the fluid to the body (when $C_{L_v} > 0$) and vice versa (when $C_{L_v} < 0$). Its behaviour is illustrated in Fig. 3 (right) for $A/D = 0.5$ and $f_0/f_s = 0.6$, 0.9, 1.1 and 1.3: C_{L_v} is negative at every spanwise location, with the most negative values occurring in the lower part of the geometry ($s/D > 10$) where the total lift coefficient reaches the highest magnitude. Therefore, this region acts as a hydro-dynamic damper to the whole structure, preventing the top part to be excited by the vortex shedding (with the only exception of the case at $f_0/f_s = 1.3$, where C_{L_v} is mildly positive for $0 < s/D < 3$). As the frequency ratio is decreased from 1.3 to 0.6, the value of C_{L_v} in the lower region increases but it does not become positive; at the same time the value at the top decreases slightly. For all the frequencies tested at this amplitude, the integral of the energy transferred along the whole span is found to be negative. For $\theta > 45^\circ$ (corresponding to $s/D \approx 10$), the axial component of the incoming velocity is significantly greater than the normal one and therefore this region shows similarities to a slender body, becoming entirely parallel to the inflow direction in the horizontal addition: following the ''Independence Principle'', the pressure field and hence the pressure force in this region appear to be

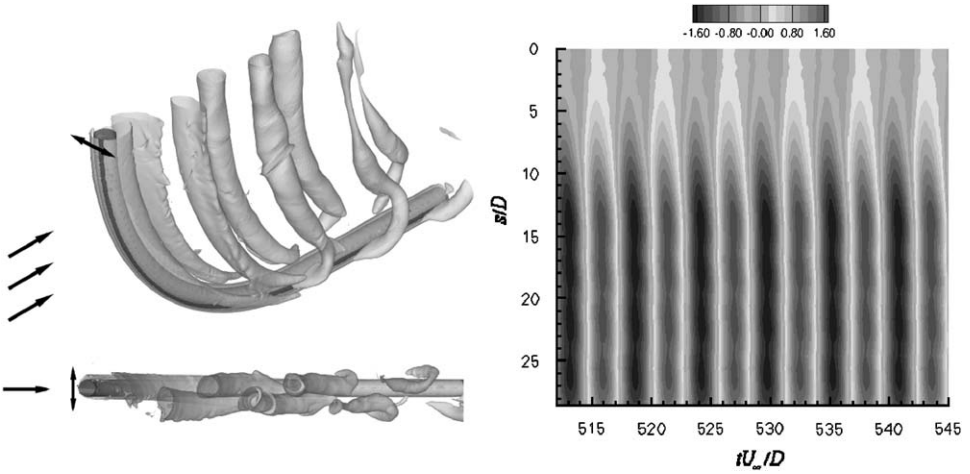

Fig. 2. Left: Wake topology for the flow past the convex configuration at $f_i = 1.1f_s$ and $A/D = 0.5$ (Re = 100); iso-surfaces at $\lambda_2 = -0.1$ and $tU_\infty/D = 524.5$. Right: Time evolution of the sectional lift coefficient along the cylinder span.

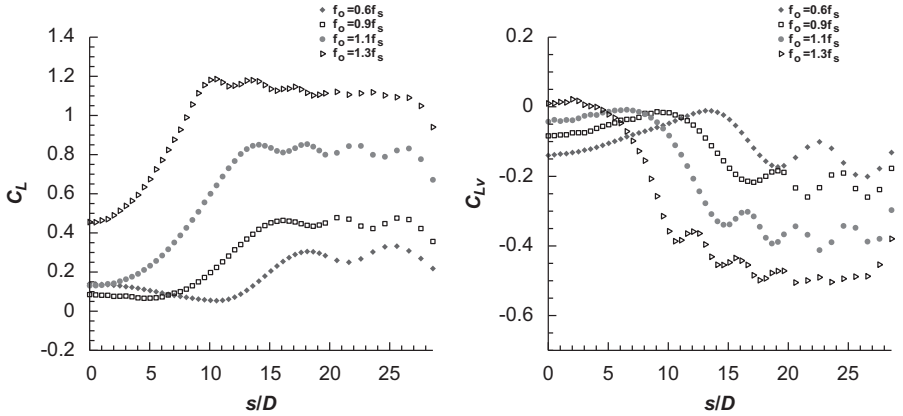

Fig. 3. Spanwise distribution of the total lift coefficient C_L (left) and of the lift coefficient in phase with the body's velocity C_{L_v} (right) at $A/D = 0.5$ and different input frequencies (Re = 100).

insensitive to the axial velocity component. Fig. 3 (left) clearly shows the predominance of the force contribution arising from this lower portion of the body; the force coefficient increases and its peak shifts to the middle region ($s/D = 10$) as the input frequency is increased. However, due to the alignment of the body with respect to the flow direction, this is a spanwise "drag-type" of force, whose magnitude and frequency are well predicted by Morison's equation based on mean in-line force coefficients in the direction of the cross-flow. The force given by Morison's equation for an oscillating cylinder in a stationary flow with Keulegan–Carpenter number KC $= \pi$ and Stokes parameter $\beta = 18.04$ isdisplayed in Fig. 4 together with the lift signal at $s/D = 26.6$. The coefficients used to calculate the lift force in the horizontal extension can be found in Bearman et al. (1985) and are given as

$$C_M = 1 + 4(\pi\beta)^{-1/2}, \quad C_D = \tfrac{3}{2}\pi^3 KC^{-1}(\pi\beta)^{-1/2}.$$

3.2. Vortex shedding outside the two-dimensional lock-in region

Simulations of the vortex shedding at very low frequencies were performed at $A/D = 0.5$ and Re $= 100$. The pair of input parameters ($f_0/f_s = 0.6, A/D = 0.5$) lies outside of the "conventional" lock-in region depicted in Fig. 1 (left) (where the frequency ratio in the x-axis is given as f_s/f_0). The λ_2 iso-surfaces and the spanwise distribution of the sectional lift coefficient are presented in Fig. 5. Similar to the shedding at higher frequencies, it is the lower part of the geometry that influences the energy transfer mechanism, preventing this configuration to be excited by the flow: however, the magnitude of C_L and C_{L_v} for $s/D<10$ is now comparable to the one in the upper half of the body, as displayed in Fig. 3.

The lift distribution along the span highlights the presence of vortex dislocations at $s/D = 10$, which result from the competition between the frequencies at the top and at the lower half of the cylinder: the region $0<s/D<10$ tends to shed vortices with a straight core at the higher frequency f_{top}, whereas for $s/D<10$ the effect of curvature prevails and the cores are bent and shed at the imposed frequency (f_{bottom}). Subsequently, at t_1 in Fig. 5 (right), f_{top} is prevailing and the cylinder sheds a straight vortex that detaches from the shear layer at about $s/D = 10$, giving rise to a dislocation. At t_2 in the following cycle, when the influence from the bottom part is predominant, a pair of curved vortices is shed in the fashion described in Section 3.1. However, these two types of cores do not have the same strength, as the level of vorticity in the curved core is significantly higher: the vorticity in the straight core is not sufficiently concentrated to cut off the supply of circulation to the forming vortex on the opposite side and this weaker core detaches once the cylinder's motion changes direction, without interaction with the opposite shear layer. This weak form of shedding is illustrated through iso-contours of spanwise vorticity in Fig. 6 (left), while the curved vortex shedding dynamics is visualised in Fig. 6 (right). The wake topology past the top sections is similar to a 2P mode, with two counter-rotating vortex pairs shed per cycle, as described by Williamson and Roshko (1988). However, a closer analysis reveals that the vorticity distribution in this "weak" type of shedding is different from the one in the 2P mode: here the two vortices that form the pair maintain the same vorticity sign in each shed pair (i.e. the first is positive and the second is negative in every pair, as shown in Fig. 6 (left)). This is consistent with the idea that the Strouhal frequency f_s is trying to re-assert itself in this region of the cylinder, which therefore tends to shed vortices at a frequency that is nearly double the frequency imposed.

3.3. Effect of the amplitude variation on the energy transfer mechanism

At lower amplitudes, the influence of the horizontal extension is weakened and the shedding from the upper half of the cylinder is stronger. Two distinct trends for the lift coefficient are found to occur depending on the frequency ratio value. At $f_0/f_s = 0.9$, the lift coefficient still reaches its maximum value in the lower part of the body, as shown in Fig. 7: however, when the amplitude of oscillation is reduced, the peak shifts further along the span, until for $A/D = 0.1$ it occurs at $s/D \approx 12$. At the same time, C_{L_v} in the range $0<s/D<12$ becomes positive for $A/D = 0.1$ and 0.25, with a maximum at $s/D = 9$. This suggests that the region of the body's span that determines the direction of the energy transfer is located in the middle part of the quarter ring. The spanwise location of the maximum C_{L_v} appears to be the same at all the amplitudes tested (see Fig. 7 (right)), suggesting that it may depend on the frequency only.

At $f_0/f_s = 1.1$, the part of the lift coefficient in phase with the velocity sharply increases: Fig. 8 shows that the maximum positive value for C_{L_v} at $A/D = 0.1$ and 0.25 is now reached in the top sections ($0<s/D<6$), as opposed to $f_0/f_s = 0.9$ where the peak in C_{L_v} occurs in the middle part of the quarter ring. Similarly, at these lower amplitudes, the total lift coefficient attains a maximum for $s/D>10$: the direction of the energy transfer is thus determined in the upper half of the body.

The net energy transfer for the whole structure is positive for ($A/D = 0.1, f_s/f_0 = 0.9$), ($A/D = 0.1, f_s/f_0 = 1.1$) and ($A/D = 0.1, f_s/f_0 = 1$): although the exact boundaries for the excitation region in the parameter plane have not been

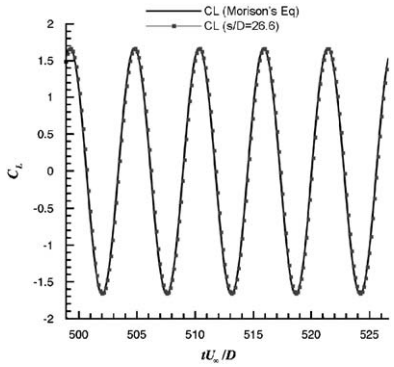

Fig. 4. Lift signal for $A/D = 0.5$ and $f_0/f_s = 1.1$ at a section $s/D = 26.6$ (horizontal extension) and force signal given by Morison's equation.

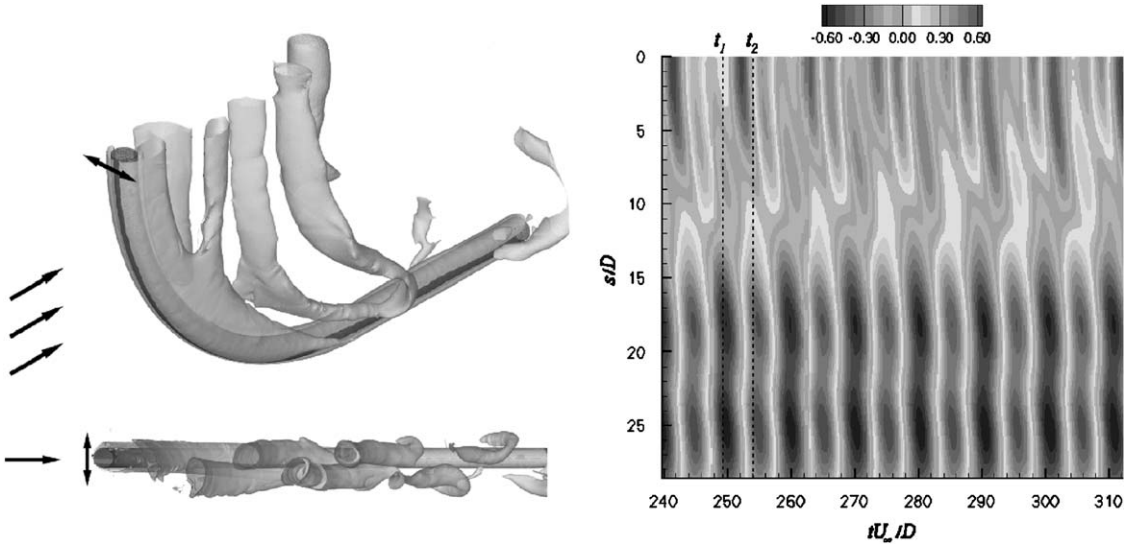

Fig. 5. Left: Wake topology for the flow past the convex configuration at $f_0 = 0.6f_s$ and $A/D = 0.5$ (Re = 100); iso-surfaces at $\lambda_2 = -0.07$ and $tU_\infty/D \approx t_1$. Right: Time evolution of the sectional lift coefficient along the cylinder span.

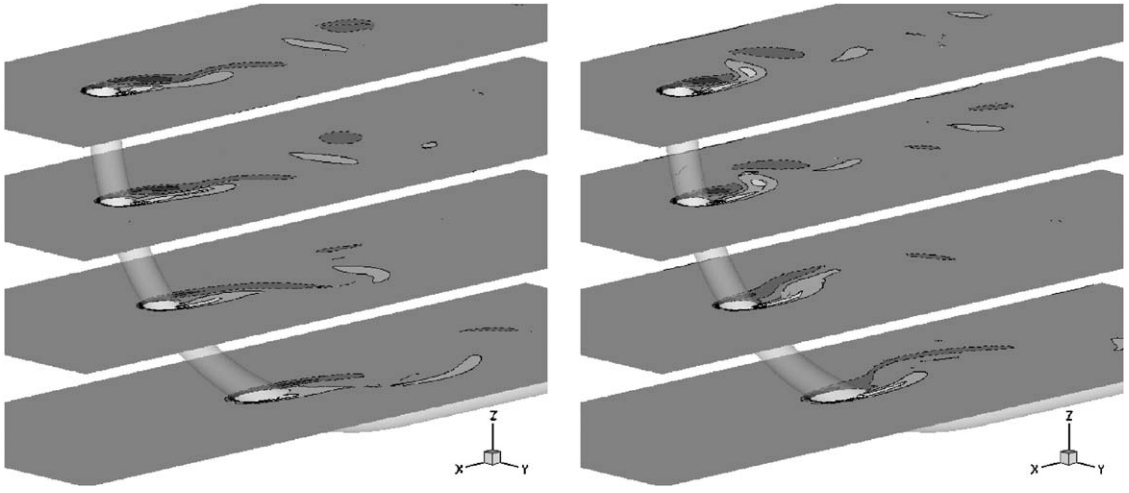

Fig. 6. Case at ($f_0/f_s = 0.6, A/D = 0.5$): spanwise vorticity at $t_1 = 249.2$ ($y = 0.5$), when the straight vortex core is shed (left), and at $t_1 = 254$ ($y = -0.5$), when the curved vortex core is shed (right). Dashed lines for negative vorticity.

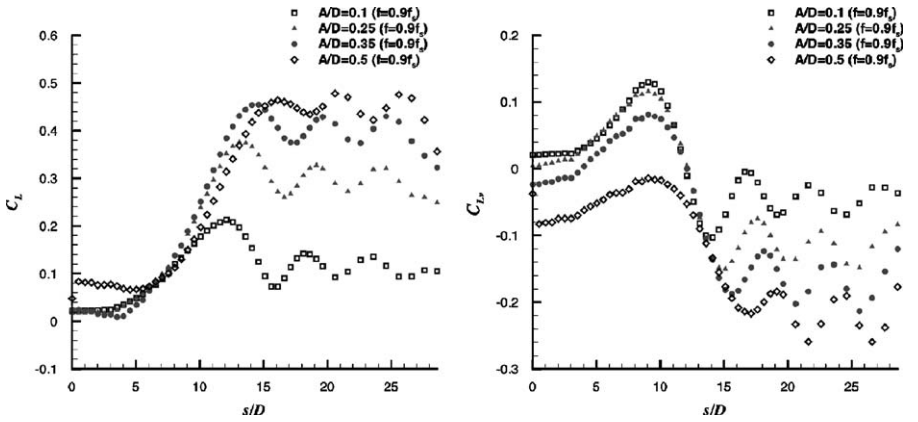

Fig. 7. Spanwise distribution of the total lift coefficient C_L (left) and of the lift coefficient in phase with the body's velocity C_{L_e} (right) at $f_0/f_s = 0.9$ and different amplitudes of oscillation (Re = 100).

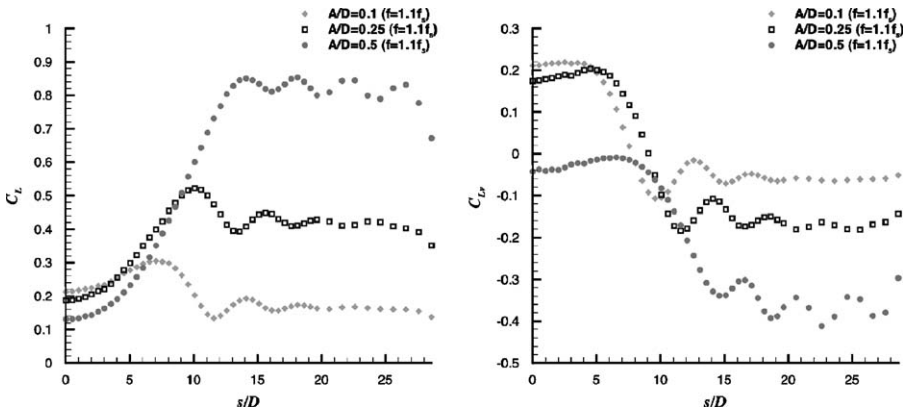

Fig. 8. Spanwise distribution of the total lift coefficient C_L (left) and of the lift coefficient in phase with the body's velocity C_{L_e} (right) at $f_0/f_s = 1.1$ and different amplitudes of oscillation (Re = 100).

determined, these results show that the excitation region for this configuration is considerably contracted when compared to its two-dimensional counterpart.

4. Vortex dislocations

As discussed in Section 3.2, the three-dimensionalities introduced by the body's curvature may lead to the occurrence of dislocations in the wake: this is particularly evident at low values of excitation frequencies, in regions of the $(A/D, f_0/f_s)$ plane outside the lock-in boundaries. This phenomenon has also been observed at low amplitudes of oscillation: for $A/D = 0.1$ and excitation frequencies below the Strouhal value, two distinct shedding frequencies were observed along the span of the cylinder, i.e. a higher frequency in the top part of the quarter ring (f_{top}) and a lower frequency corresponding to the imposed frequency for the forced vibration in the lower region (f_{bottom}). Vortex dislocations are periodically formed in the wake as these cells move out of phase with each other. Consistent with findings in past literature on shedding at low Reynolds numbers (Williamson, 1992), their occurrence is found to be periodic in time and at fixed positions along the span, as shown by the spanwise iso-contours of C_L in Fig. 9 for $f_0/f_s = 0.7$, 0.8 and 0.9. In all of these three cases, the dislocation is characterised by a beat frequency $f_D = f_{\text{top}} - f_{\text{bottom}}$. When the imposed frequency is increased from $0.7f_s$ to $0.9f_s$, the dislocation position shifts towards the top of the cylinder and its frequency f_D decreases. It should be noted that the imposed frequency always corresponds to the value f_{bottom} found at $s/D > 12$ approximately.

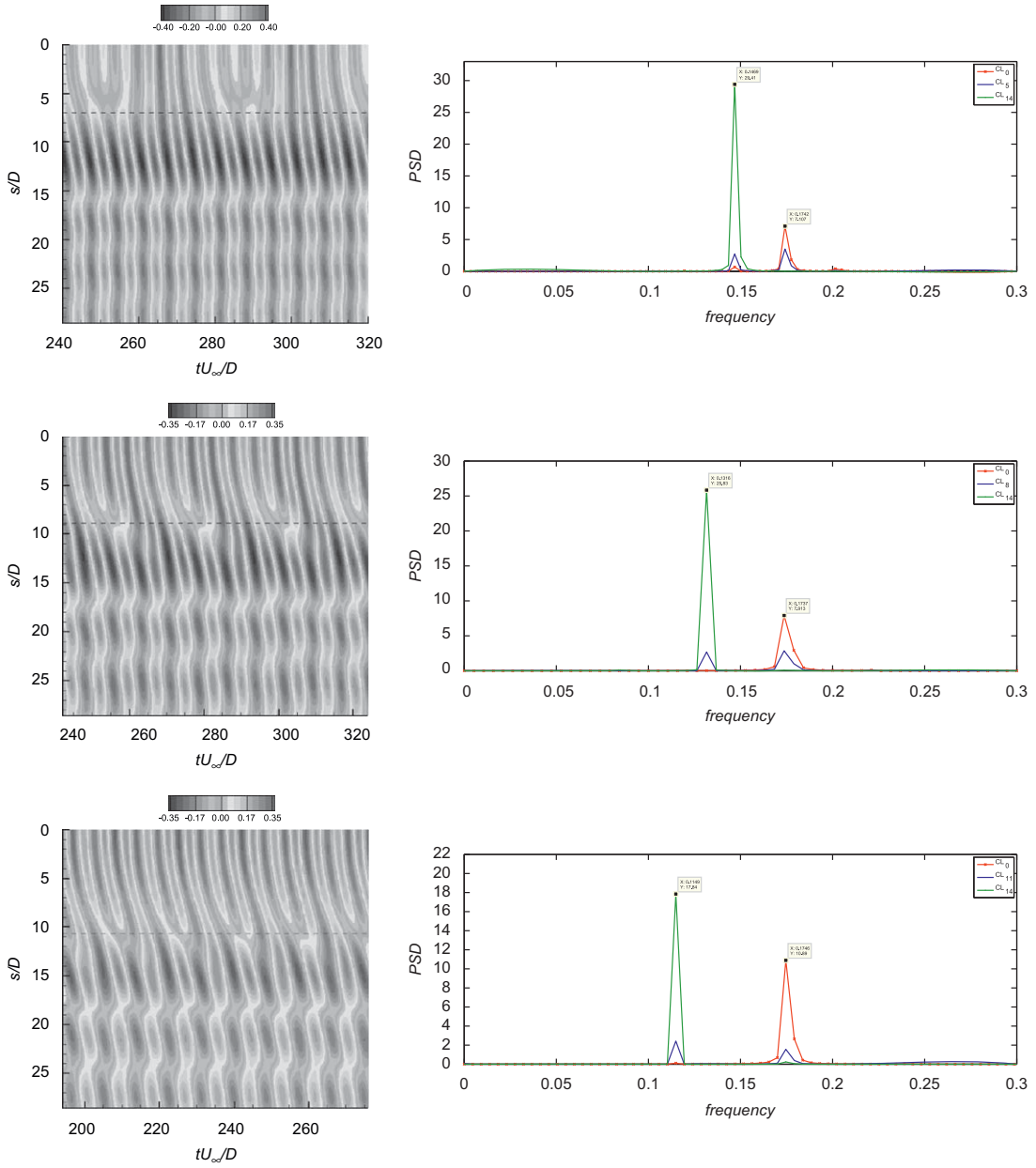

Fig. 9. Left: Spanwise distribution of the total lift coefficient C_L at $A/D = 0.1$ and $f_0/f_s = 0.9$, 0.8 and 0.7 (top to bottom). Right: Dominant frequencies at three different spanwise locations, namely in the top part, at the dislocation position and in the bottom part of the quarter ring.

Williamson (1992) analysed the natural and forced formation of vortex dislocations in the laminar regime and used a small ring disturbance to trigger this mechanism at a local spanwise position; the dislocation frequency was found to decrease with decreasing ring diameter. In the curved cylinder there is no such disturbance; however, if we consider two-dimensional sections in the plane (x, y) placed at different spanwise locations, the local cross-section of the body is an ellipsis whose greater diameter is larger than the cylinder diameter D: similar to the ring diameter in Williamson's experiments, this introduces a different length-scale in the problem. An approximate relationship between the ratio of the dislocation frequency to the primary vortex shedding frequency and the greater diameter of the elliptical cross-section D_e was found to hold for the cases presented in Fig. 9. This is given as $f_D/f_0 = D_e/D - 1$. Substituting the oscillation frequency f_0 and the dislocation frequency f_D, this equation provides a value for D_e that identifies the

cross-sectional plane at which the dislocation is expected to occur: for the three frequencies presented in Fig. 9, $f_0/f_s = 0.7$, 0.8 and 0.9, the nondimensional arc-lengths corresponding to the evaluated elliptical diameter are $s/D = 10.6$, 8.9 and 7, respectively (as indicated by the dashed line in the lift iso-contour plots). This is in agreement with the value at the lower boundary of the dislocation highlighted by the lift iso-contours in Fig. 9 (left), where the vortex splitting takes place.

A further observation which supports this interpretation may be derived from the existence of a mathematical relationship that allows the oblique-shedding Strouhal data St_θ to collapse onto the parallel-shedding Strouhal curve St_0, hence giving rise to an universal St/Re curve. Williamson (1989) provides experimental evidence that such a relationship exists in the form $\mathrm{St}_0 = \mathrm{St}_\theta/\cos\theta$, where θ is the angle of oblique shedding. If we consider the shedding form the top of the body to be nearly parallel to the cylinder's axis in the upper half of the quarter ring and the bent cores in the lower part to be at an oblique angle θ dependent on the nondimensional arc-length at which the dislocation occurs, a similar relationship can be given as

$$f_{\mathrm{top}} = f_{\mathrm{bottom}}/\cos\theta. \tag{1}$$

Substituting the value of the frequencies found by means of the spectral analysis (see Fig. 9 (right)), Eq. (1) leads to a value for θ which identifies the same spanwise positions for the dislocation given by the argument of the elliptical cross-sections illustrated above.

5. Conclusions

Fully three-dimensional forced vibration simulations have been performed to investigate the complex vortex dynamics past a curved convex cylinder in the laminar shedding regime.

The difference between $C_{L_{\mathrm{top}}}$ and $C_{L_{\mathrm{bottom}}}$ increases with the frequency ratio f_0/f_s for a fixed amplitude of $0.5D$. A similar trend is found when the amplitude of motion is increased at fixed frequency ratios equal to 0.9 and 1.1. At higher amplitudes, the dampening influence stemming from the extension propagates towards the top region when the imposed frequency is increased, resulting in a negative energy transfer for the whole geometry: the lower part of the body is therefore predominant at these amplitudes. This region behaves like a slender body oscillating in a uniform flow and undergoes a spanwise "drag-type" of force, which can be correctly predicted by Morison's equation. However, when the oscillation amplitude is reduced to $0.1D$ and $0.25D$, C_{L_v} shifts towards positive values and an excitation region can be identified. Its extension appears significantly contracted when compared to that of the two-dimensional cylinder. At these lower amplitudes, the energy transfer mechanism is found to be primarily influenced by the middle region (at $f_0/f_s = 0.9$) and by the top region (at $f_0/f_s = 1.1$). A similar result was obtained by De Vecchi et al. (2007), when the convex configuration was forced to transversely rotate about the axis of the horizontal extension, which was therefore kept fixed.

When the frequency ratio is chosen outside the lock-in region ($A/D = 0.5, f_0/f_s = 0.6$), a "weak" form of shedding appears at the top sections. Its occurrence is related to the competition between two frequencies: the upper half of the body sheds two pairs of straight vortices per cycle at a frequency close to the Strouhal value, while curved cores detach from the lower region in a 2S mode at the imposed frequency. Vortex dislocations are observed in the middle of the quarter ring at $\theta \approx 45^\circ$. This phenomenon also occurs at low amplitudes; similar to the case at ($A/D = 0.5, f_0/f_s = 0.6$), the dislocations result from competing frequencies in the different regions of the span and take place at a beat frequency $f_D = f_{\mathrm{top}} - f_{\mathrm{bottom}}$. They occur periodically and at fixed spanwise positions; as the imposed frequency is increased and the amplitude is kept fixed at $A/D = 0.1$, their location moves towards the top of the body and their frequency f_D decreases. When $f_0 > f_s$, they disappear and the shedding is again governed by the middle/lower part of the body; this is consistent with the findings of Nuzzi et al. (1992), who observed an alternation of split and "unsplit" vortices only at low frequencies. This shift in the spanwise position of the dislocation is associated with the introduction of different length-scales in the problem, as a result of the body's curvature. A qualitative argument based on the mathematical relationship proposed by Williamson (1992) appears to support this conclusion.

From an energy point of view, the presence of a dislocation gives rise to a "pocket" of excitation just below the dislocation point: C_{L_v} reaches its maximum at the same value of s/D at which the dislocations occur and its peak value increases with the spanwise extension of the dislocation.

Acknowledgements

The authors would like to acknowledge the financial support provided by the Engineering and Physical Sciences Research Council (UK). A.d.V. also wishes to acknowledge the Royal Academy of Engineering (UK), who supported part of her attendance to the 5th BBVIV Conference.

References

Bearman, P., Downie, M., Graham, J., Obasaju, E., 1985. Forces on cylinders in viscous oscillatory flow at low Keulegan–Carpenter numbers. Journal of Fluid Mechanics 154, 337–356.

Blackburn, H., Govardhan, R., Williamson, C., 2000. A complimentary numerical and physical investigation of vortex-induced vibration. Journal of Fluids and Structures 15, 481–488.

Blackburn, H., Henderson, R., 1999. A study of two-dimensional flow past an oscillating cylinder. Journal of Fluid Mechanics 385, 255–286.

De Vecchi, A., Sherwin, S., Graham, J., 2007. Wake dynamics of external flow past a curved circular cylinder with the free-stream aligned to the plane of curvature. In: Proceedings of the IUTAM Symposium on Unsteady Separated Flows and their Control, Greece.

Eisenlohr, H., Ecklemann, H., 1989. Vortex splitting and its consequences in the vortex street wake of cylinders at low Reynolds number. Physics of Fluids A 1, 189–192.

Govardhan, R., Williamson, C., 2000. Modes of vortex formation and frequency response of a freely vibrating cylinder. Journal of Fluid Mechanics 420, 85–130.

Karniadakis, G.E., Israeli, M., Orszag, S.A., 1991. High-order splitting methods for the incompressible Navier–Stokes equations. Journal of Computational Physics 97, 414–443.

Karniadakis, G.E., Sherwin, S.J., 2005. Spectral/hp Element Methods for CFD. Oxford University Press, Oxford.

Leontini, J., Stewart, B., Thompson, M., Hourigan, K., 2006. Wake state and energy transitions of an oscillating cylinder at low Reynolds number. Physics of Fluids 18, 067101.1–067101.9.

Meneghini, J., Bearman, P., 1995. Numerical simulations of high amplitude oscillatory flow about a circular cylinder. Journal of Fluids and Structures 9, 435–455.

Miliou, A., de Vecchi, A., Sherwin, S.J., Graham, J.M.R., 2007. Wake dynamics of external flow past a curved cylinder with the free-stream aligned to the plane of curvature. Journal of Fluid Mechanics 592, 89–115.

Nuzzi, F., Magness, C., Rockwell, D., 1992. Three-dimensional vortex formation from an oscillating, non-uniform cylinder. Journal of Fluid Mechanics 238, 31–54.

Ponta, F., Aref, H., 2005. Vortex synchronization regions in shedding from an oscillating cylinder. Physics of Fluids 17, 011703.

Ponta, F., Aref, H., 2006. Numerical experiments on vortex shedding from an oscillating cylinder. Journal of Fluids and Structures 22, 327–344.

Willden, R., McSherry, R., Graham, J., 2008. Prescribed cross-stream oscillations of a circular cylinder at laminar and early turbulent Reynolds numbers. In: Proceedings of the Fifth Bluff Bodies and Vortex-Induced Vibration Conference, Brazil.

Williamson, C., Roshko, A., 1988. Vortex formation in the near wake of an oscillating cylinder. Journal of Fluids and Structures 2, 355–381.

Williamson, C., 1988. Defining a universal and continuous Strouhal–Reynolds number relationship for the laminar vortex shedding of a circular cylinder. Physics of Fluids 31, 3165.

Williamson, C., 1989. Oblique and parallel modes of vortex shedding in the wake of a circular cylinder at low Reynolds numbers. Journal of Fluid Mechanics 206, 579–627.

Williamson, C., 1992. The natural and forced formation of spot-like 'vortex dislocations' in the transition of a wake. Journal of Fluid Mechanics 243, 393–441.